Waveguide-integrated silicon T centres

A. DeAbreu,[1,2] C. Bowness,[1,2] A. Alizadeh,[1,2] C. Chartrand,[1,2] N. A. Brunelle,[1,2] E. R. MacQuarrie,[1,2] N. R. Lee-Hone,[2] M. Ruether,[1,2] M. Kazemi,[1,2] A. T. K. Kurkjian,[2] S. Roorda,[3] N. V. Abrosimov,[4] H.-J. Pohl,[5] M. L. W. Thewalt,[1] D. B. Higginbottom,[1,2] AND S. Simmons[1,2,*]

[1]*Department of Physics, Simon Fraser University, Burnaby, BC V5A 1S6, Canada*
[2]*Photonic Inc., Coquitlam, BC, Canada*
[3]*Département de physique, Université de Montréal, Montréal, QC H3C 3J7, Canada*
[4]*Leibniz-Institut für Kristallzüchtung, 12489 Berlin, Germany*
[5]*VITCON Projectconsult GmbH, 07745 Jena, Germany*
[*]*s.simmons@sfu.ca*

Abstract: The performance of modular, networked quantum technologies will be strongly dependent upon the quality of their quantum light-matter interconnects. Solid-state colour centres, and in particular T centres in silicon, offer competitive technological and commercial advantages as the basis for quantum networking technologies and distributed quantum computing. These newly rediscovered silicon defects offer direct telecommunications-band photonic emission, long-lived electron and nuclear spin qubits, and proven native integration into industry-standard, CMOS-compatible, silicon-on-insulator (SOI) photonic chips at scale. Here we demonstrate further levels of integration by characterizing T centre spin ensembles in single-mode waveguides in SOI. In addition to measuring long spin T_1 times, we report on the integrated centres' optical properties. We find that the narrow homogeneous linewidth of these waveguide-integrated emitters is already sufficiently low to predict the future success of remote spin-entangling protocols with only modest cavity Purcell enhancements. We show that further improvements may still be possible by measuring nearly lifetime-limited homogeneous linewidths in isotopically pure bulk crystals. In each case the measured linewidths are more than an order of magnitude lower than previously reported and further support the view that high-performance, large-scale distributed quantum technologies based upon T centres in silicon may be attainable in the near term.

1. Introduction

Drawing inspiration from classical information processing, *modular* quantum information architectures offer a clear path to large-scale quantum computers and quantum networks. Breaking the constraints of local processors by networking will unlock the full competitive advantage of quantum computing technology. Towards this end, a number of modular quantum architectures have been proposed [1–3] and small-scale demonstrations have been realised [4–6].

Abstractly, the ideal modular quantum architecture simultaneously offers long-lived, high-fidelity qubits as well as direct photonic access to efficiently distribute entanglement across the network. Quantum objects known as spin-photon interfaces offer all of these capabilities in a single element. Examples include trapped ions [1,4] and neutral atoms [7], but importantly also solid-state systems such as integrated quantum dots [8–12], rare earth ions [13–16] and colour centre defects within group-IV crystals (diamond [17,18], SiC [19–21], and Si [22–24]).

Commercial constraints will affect the pace with which these modular technologies move from small-scale demonstrations to practical deployment. In this context, the ideal quantum

architecture communicates via telecommunications-band photons without any transduction [25], and leverages the manufacturing expertise of the semiconductor industry, and in particular silicon, which is the dominant host platform for integrated photonics and electronics manufacturing. If realised, such an architecture could simultaneously underpin global quantum communications using terrestrial repeaters [26] as well as distributed modular quantum computers, all leveraging the same shared core quantum element.

Opportunities to realise such an architecture have sparked considerable, but only very recent, interest in telecommunications-band colour centres directly embedded within silicon. There have been three categories of focus: (1) bright emitters without ground state spins, such as the G [27–30], C [31], and W [32,33] centres, (2) dim yet high-efficiency emitters with optical access to spins such as erbium [22,29,34,35], and (3) the T centre, which offers relatively bright photon emission as well as direct access to long-lived spins. The T centre was first assessed and proposed as a competitive candidate quantum spin-photon interface in 2020 [24]. Integration tests quickly followed, establishing that T centre qubits could be created at high densities [36] and individually addressed at scale in industry-standard silicon-on-insulator (SOI) [37].

Although the T centres in these demonstrations possessed many encouraging features, it was unclear if their optical properties were sufficient to support optically-generated entanglement for quantum networking and modular quantum processors. Spin-photon interfaces may be entangled by emission [38] or reflection-based [39,40] protocols. Emission-based protocols require that the ratio of homogeneous and lifetime-limited linewidths is close to one [41,42]. In general this 'transform limit' may be reached by utilizing optical resonators to Purcell enhance the emission and increase the lifetime-limited linewidth accordingly [14,43,44]. Similarly, reflection-based protocols using high-cooperativity emitter-cavity coupling require that the homogeneous linewidth is small compared to this emitter-cavity coupling. In both cases the homogeneous linewidth critically determines the optical resonator quality required for high fidelity entanglement, and for T centres the relevant homogeneous linewidth remained unknown.

In this work we study the optical and spin properties of T centres in integrated silicon photonic waveguides, the fundamental building block of an on-chip optical network. We fabricate single-mode waveguides containing ensembles of T centres and measure their key optical properties. We find remarkably sharp homogeneous linewidths that will support remote entanglement generation via an emission-based entanglement scheme with modest Purcell enhancements. We compare these linewidths with new measurements in bulk ^{28}Si and report near-transform-limited optical transitions. Finally, we place our integrated sample in a magnetic field and use hole burning to initialize and readout the spin states and report competitive spin T_1 lifetimes. Taken together, these results showcase the T centre as a promising candidate for a modular quantum information architecture.

2. T centre

The T centre is a multi-component colour center in silicon, possessing a bound exciton optical transition at 1326 nm (935 meV), in the telecommunications O-band [24]. Known for many years as a defect in the class of radiation damage centres, many of the T centre's properties had been known previous to its rediscovery as a qubit candidate [45,46]. The proposed chemical structure [45], shown in Fig. 1(b), comprises two inequivalent carbon atoms and a hydrogen atom, and possesses an unpaired electron in the ground state with an isotropic Landé g-factor [24]. In the excitonic ground state the electron of the bound exciton forms a singlet with this ground state electron. The expected fourfold degeneracy of the spin-3/2 hole is lifted by the reduced symmetry of the T centre, resulting in a spin-1/2 doublet ground state for the bound exciton, TX_0, and a higher energy doublet, TX_1, 1.76 meV above TX_0.

The TX_0 to ground state transition was determined to have a lifetime of 0.94 ± 0.01 µs and a Debye-Waller factor of 0.23 ± 0.01 [24]. The radiative efficiency is not precisely known,
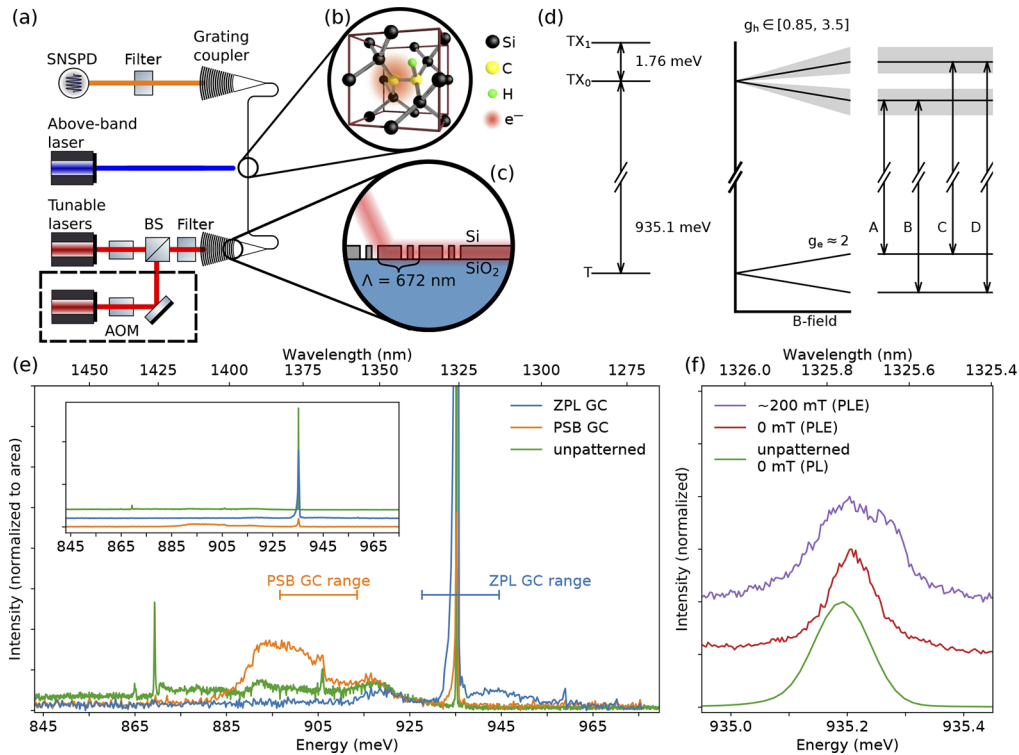
Fig. 1. T centre waveguide integration and optical spectra. (a) Experimental setup for measuring T centre ensembles within integrated waveguide devices (not to scale) illustrating the two excitation pathways: above-bandgap excitation from above the chip (450/980 nm, blue) and resonant excitation through a GC and waveguide (1326 nm, red). An optional second resonant laser is available. Luminescence from the phonon sideband ($\sim$ 1375 nm, orange) is directed to a superconducting nanowire single photon detector (SNSPD). **(b)** The proposed chemical structure of the T centre. **(c)** A side-on schematic of the subwavelength grating coupler showing the period of the ZPL GC. **(d)** Energy level diagram of the T centre under a magnetic field. Grey fill indicates the range of possible g_h values. **(e)** PL spectra from CW above-bandgap excitation measured through the two GC ports in addition to a PL spectrum from an identical unpatterned sample. The nominal wavelength ranges (two-σ) of the zero-phonon line and phonon sideband grating couplers are marked by horizontal bars. **(f)** PLE spectra of the TX_0 ZPL line for the same device both in a magnetic field and at zero field compared to the PL of the unpatterned material.

with theoretical estimates in the range 0.19–0.72 [47] and an experimental lower bound of 0.03 [37]. Thermal activation from TX_0 to TX_1 was found to freeze out below ~ 2 K resulting in low temperature inhomogeneous linewidth of 6.5 ± 0.2 GHz for silicon with a natural isotopic abundance and 33 ± 2 MHz for isotopically purified ^{28}Si [24].

Spectroscopy at magnetic fields revealed 12 inequivalent sets of 24 possible T centre orientations. The ground state electron Landé g-factor was found to be isotropic with a value of 2.005 ± 0.008 whereas the hole g-factor was found to be very anisotropic, ranging between 0.85–3.5, depending on the magnetic field axis relative to the axis of the orientational subset [24,36]. Furthermore, the ground state level structure was determined to feature an anisotropic hyperfine coupling between the electron and the spin-1/2 hydrogen nucleus with an effective hyperfine splitting <5 MHz.

3. T centre waveguide devices

We generate T centres in a silicon-on-insulator (SOI) wafer and pattern single-mode waveguide devices (method in Supplement 1). These devices are optically addressed by an array of single-mode fibres positioned above the plane of the photonic chip, which is optionally mounted with a removable permanent magnet and cryogenically cooled to either 4.3 K or 1.2 K (method in Supplement 1). Each device is a 360 μm long single-mode strip waveguide, terminated by two sub-wavelength grating couplers (GCs) [48], shown schematically in Fig. 1(a), (c). The two GCs are designed for different wavelengths, one centred on the T centre zero-phonon line (ZPL) and one red-shifted GC that covers a portion of the phonon sideband (PSB) spectrum. This configuration allows for resonant excitation of the TX_0 ZPL through one GC port and detection of phonon sideband fluorescence through the other. The sample can be resonantly excited with one or two, independently pulsed, tunable lasers. Emission is collected from the PSB GC and directed to an external superconducting nanowire single photon detector (SNSPD) after a 1340 nm longpass filter to further reject the excitation laser. An additional fibre port directly above the waveguide centre can be used for direct, above-bandgap excitation of the waveguide itself, with fluorescence collected from either/both of the PSB or ZPL GC ports; in this case no filter is necessary and the fluorescence is sent to an optical spectrometer (see Supplement 1 Methods).

4. PL and PLE

We first demonstrate T centres within the waveguide by photoluminescence (PL) spectroscopy. Above-bandgap excitation through the middle port generates excitons that bind to centres and subsequently luminesce upon recombination. We measure the luminescence separately from the two GC ports and record spectra with an ultra low-noise optical spectrometer. Figure 1(e) shows these two PL spectra compared to a reference from an identical unpatterned SOI chip. The ZPL GC spectrum is dominated by a bright TX_0 ZPL, and the PSB GC spectrum exhibits a portion of the phonon sideband to lower energy including the distinctive TX_0 local vibrational mode (LVM) replica L_1 at 906 [24,45].

We measure the T waveguide device at higher resolution by photoluminescence excitation (PLE) spectroscopy. Figure 1(f) compares the waveguide T PLE spectrum with the unpatterned material spectrum from Fig. 1(e) in the vicinity of the TX_0 ZPL. The resulting zero-field PLE spectrum is typical of an inhomogeneous ensemble. Concentration estimates on similar material [37] suggest that each waveguide device contains upwards of 600 centres. Resonant excitation through the ZPL GC illuminates a single linearly polarized waveguide mode. The inhomogeneous distribution of the T centre ensemble within this mode is 22.7 ± 0.3 GHz (0.0939 ± 0.0012 meV). Reference [36] determined that both implantation damage and strain from the silicon to silicon oxide interface [49] contribute inhomogeneous broadening in SOI ensembles (increasing linewidth from the mass homogeneity limit of 6.5 GHz [24] to ~ 20 GHz). The pre-fabrication linewidth of this SOI material was slightly larger, 27.3 ± 0.2 GHz (0.1129 ± 0.00008 meV). In contrast to the micropuck-integrated T centres of Ref. [37], the waveguide ensemble linewidth is

lower than the unpatterned material, indicating that the TX_0 energy of centres in this mode at the centre of the device layer is insensitive to waveguide fabrication. Fabricating devices may even release strain from the SOI chip [28].

5. Lifetime measurements

We measure the average excited state lifetime of this waveguide-coupled ensemble and find that it is not dramatically different from the bulk crystal, but the precise value depends on the excitation method. First, we measure the lifetime with above-bandgap excitation through the middle fibre using a 965 nm pulsed laser. The transient fluorescence, shown in Fig. 2, decays exponentially with a lifetime of 0.96 ± 0.01 µs, consistent with the equivalent bulk above-bandgap excitation lifetime of 0.94 ± 0.01 µs [24]. We conclude that there is no evidence of Purcell enhanced or suppressed emission within this measurement uncertainty (simulated waveguide Purcell factors are included as SI).
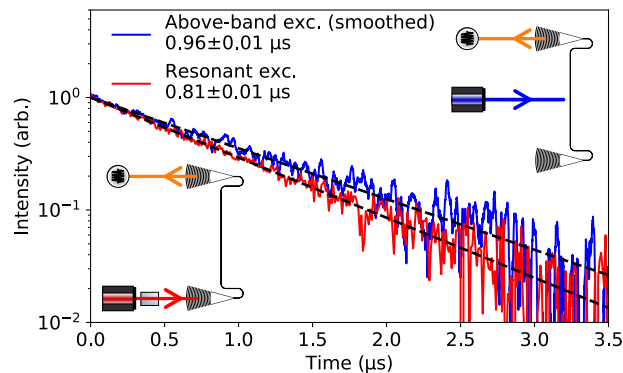

Fig. 2. Lifetime measurements. Luminescence lifetime from the two excitation pathways: pulsed above-bandgap light coupled from above (blue, upper right inset) and pulsed resonant light coupled through the waveguide (red, lower left inset). Both curves are fit with an exponential decay.

When exciting resonantly through the waveguide we measure a lifetime of 0.81 ± 0.01 µs, 16% lower than the above-bandgap excitation value. Additional measurements to investigate this discrepancy are included as Supplementary Information. The excited state lifetime shows no dependence on the resonant excitation power (Supplement 1Fig. S4(a)) indicating that stimulated emission is negligible. Furthermore, the simulated waveguide Purcell enhancement cannot account for this difference in lifetimes under reasonable assumptions (Supplement 1Fig. S4(c–e)). The difference may instead be due to the free exciton capture time or superradiant enhancement [50,51].

6. Spectral hole burning

An emitter's homogeneous linewidth is a critical metric for entangling and networking spin-photon qubits [52]. An ideal emitter will have a lifetime-limited linewidth, however this deteriorates with dephasing and spectral diffusion due to environmental fluctuations. In the case of the T centre, the lifetime-limited linewidth is 170 kHz. In Ref. [36] the *long-time* homogeneous linewidth of unpatterned SOI with the same T centre recipe was determined to be 1.3 ± 0.3 GHz, limited by 'slow' spectral diffusion (SD) on timescales much longer than the excited state lifetime. Similar long-time homogeneous linewidth values for single-T centres were measured by Ref. [37]. Such slow SD can be overcome with a feedback mechanism that tunes wandering emitters back into mutual resonance [53,54]. Dephasing and 'fast' SD (on the timescale of the emission lifetime)

on the other hand, are an intrinsic limit to emitter performance [41,52]. Here we report the first *instantaneous* homogeneous linewidth measurement of T centres. We compare the instantaneous linewidth in both waveguide devices and bulk isotopically-enriched ^{28}Si by spectral hole burning and find linewidths that are dramatically lower than the published long-time linewidths, in some cases approaching the lifetime limit, and very promising for T centre spin-photon networks.

A pump laser is tuned to the peak of the inhomogeneous linewidth and a second probe laser is swept about this wavelength. When the lasers are detuned further than a homogeneous linewidth, $\Delta\omega_{\text{hom}}$, the lasers address independent sub-ensembles of T centres and produce a fluorescence signal that is simply the sum of the emission from each sub-ensemble. When the detuning is small and the two lasers are within one homogeneous linewidth, the lasers address the same sub-ensemble and the signal is reduced due to saturation. Scanning the probe laser produces a spectrum with a 'spectral hole' at the wavelength of the pump laser, and linewidth, $\Delta\omega_{\text{hole}}$, given by:

$$\Delta\omega_{\text{hole}} = \Delta\omega_{\text{hom}} \left(1 + \sqrt{1 + \left(P_{\text{probe}} + P_{\text{pump}}\right)/P_{\text{sat}}}\right) \tag{1}$$

where P_{probe}, P_{pump}, and P_{sat} are the probe, pump, and saturation powers respectively [55]. In general $\Delta\omega_{\text{hom}} < \frac{1}{2}\Delta\omega_{\text{hole}}$.

We perform spectral hole burning on waveguide devices at 1.2 K, at zero magnetic field, at a range of pump powers, and measure an instantaneous linewidth that power broadens according to Eq. (1), shown in Fig. 3(a). Details of the method and analysis are provided as Supplement 1. The spectral hole we measure at the lowest pump power, inset to Fig. 3(a), corresponds to an instantaneous linewidth of only 67 ± 3 MHz (full width at half maximum)—an order of magnitude lower than the long-time single-T centre device linewidths measured in Ref. [37]. We note that this measurement does not attain the low power limit, as such it is an upper bound for the homogeneous linewidth. Extrapolating the fitted linewidth model to the low-power limit, we infer that the true instantaneous linewidth is 4 ± 4 MHz.

We can illustrate the impact of additional dephasing by measuring waveguide devices at an elevated temperature. At 1.2 K, thermal activation to TX$_1$ is frozen out, but at 4.3 K thermal excitation between the two excited state levels dephases the optical transition TX$_0$ [24]. We observe a minimum instantaneous linewidth of 590 ± 30 MHz at 4.3 K and once again measure optical power broadening according to Eq. (1). The inferred low-power limit is 470 ± 30 MHz, higher than the 290 MHz expected at this temperature from the model in Ref. [24]. PL spectra confirm that the TX$_0$–TX$_1$ level splitting is unchanged compared to bulk ensembles. The difference may instead be due to the altered phononic density of states within the waveguide.

The low-temperature linewidth is a significant improvement over the performance used to estimate requirements for a T centre quantum optical network in Refs. [36,37], and very promising for an integrated luminescence center with little material or fabrication process optimization yet done. The primary reason these hole burning results produce narrower linewidths than those measured in Refs. [36,37] is the measurement timescale. The burnt hole heals during the centre's excitation and decay time, approximately the excited state lifetime (<1 μs). Hole burning provides a measure of the instantaneous homogeneous linewidth depending only on dephasing and spectral diffusion from environmental fluctuations happening within this short window. The relevant timescale for Refs. [36] and [37] are, respectively, the electron spin T_1 lifetime and the measurement integration time—both much longer than 1 μs. T centre material and fabrication studies will likely achieve further reductions by removing sources of spectral diffusion, as has been seen in other materials [56,57].

We compare instantaneous linewidths before and after waveguide fabrication by performing zero-field, low-temperature hole burning on unpatterned SOI (see Supplement 1 for details). This hole burning spectrum, shown in Fig. 3(b), indicates an instantaneous linewidth less than 54 ± 1 MHz at low powers. Limited SNR prohibited a power study of the unpatterned
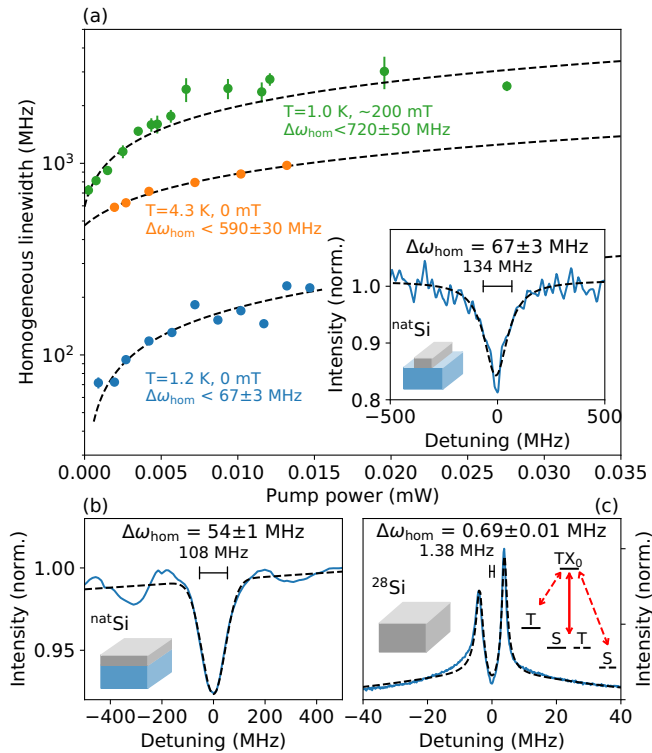
Fig. 3. Instantaneous homogeneous linewidth via hole burning. (a) Spectral hole burning in a waveguide device under various temperature and field conditions, all fit with optical pump power dependence from Eq. (1). Error bars are one-σ uncertainty ranges from an inverse-variance weighted average over fits to repeated hole-burning measurements, binned based on power. (Inset) Lowest pump power spectral hole measured at 1.2 K, zero-field. (b) Hole burning on unpatterned SOI shows only a small linewidth increase from device patterning. (c) Hole burning on bulk ^{28}Si, fit with a three level rate equation. (Inset) Triplet-singlet energy level for two sub-ensembles showing the pump-probe detunings for the anti-holes.

material, so we cannot infer the true zero-power linewidth. We observe that the lineshapes in the waveguide and unpatterned materials are different, Lorentzian and Gaussian respectively. This may indicate different spectral diffusion environments. A Lorentzian lineshape is typical [55] however Gaussian lineshapes have been seen in other solid state environments [58,59]. Nevertheless, the instantaneous linewidths are on the same order of magnitude and we see no evidence that either the electron beam lithography and etching procedure to produce waveguide devices, or the presence of new, rougher, etched silicon-air interfaces results in greater fast spectral diffusion. The resilience of T centres to integrated device environments bodes well for future work with T centres and photonic interfaces, such as the integration with nanophotonic cavities.

For comparison, we measured the hole burning spectrum of a ^{28}Si sample to obtain the linewidth in an isotopically and chemically pure environment with T centres far from surfaces. Strikingly, this instantaneous linewidth measurement approaches the T centre's fundamental lifetime-limited linewidth. An example ^{28}Si hole burning spectrum is shown in Fig. 3(c). It features two sharp peaks or 'anti-holes' with only a faint indication of a hole. This indicates that we are able to hyperpolarize into each of two long-lived ground states. We are optically

resolving, for the first time, the zero-field hyperfine splitting of the ground state [24] (illustrated in the inset of Fig. 3(c)).

A three level rate equation model was created to determine the true instantaneous linewidth from this steady-state spectrum. The full details of this model are presented in Supplement 1 which, in addition to the instantaneous linewidth, had the zero-field hyperfine splitting and the relative degeneracies of the ground states as free parameters. This model was used to simultaneously fit five hole burning spectra at different pump/probe power ratios, resulting in a triplet-singlet zero field splitting of 3.85 ± 0.01 MHz, with the triplet higher in energy than the singlet. Finally, the fit revealed a instantaneous linewidth of 0.69 ± 0.01 MHz—just 4 times larger than the lifetime-limited value of 170 kHz. Only very modest lifetime reduction would be needed to obtain transform-limited emission from this ^{28}Si base material. These measurements indicate that the T centre's instantaneous linewidth can be made much lower than previously known [24], and further improvements to the T centre implant recipe and SOI material may yield a substantial linewidth reduction.

7. Spin manipulation

In order to optically control the ensemble's electron spin state we may apply a magnetic field and split TX_0 into four spin-selective transitions A–D as per Fig. 1(d). When mounted on the permanent magnet and cooled to 1 K, we expect a ~ 200 mT magnetic field at the device position, oriented normal to the SOI sample along the $\langle 100 \rangle$ axis. In this configuration the inhomogeneous spectrum broadens to 39.6 ± 0.5 GHz (0.164 ± 0.002 meV) (Fig. 1(f)), which is not accounted for by the magnetic field alone as determined by a simulation using the rate equation model (see Supplement 1). Clamping the sample over the neodymium magnet may strain the sample and shift TX_0 across the waveguide ensemble [60,61]. At this field the ground state is split by $\Delta_g = 6$ GHz, the orientation of the field along the $\langle 100 \rangle$ axis splits the excited state by either $\Delta_e^1 = 3$ GHz or $\Delta_e^2 = 8$ GHz depending on centre orientation ($g_h^{1,2} = 0.91, 2.55$, with degeneracies 4 and 8 respectively) [36]. We therefore expect well-resolved spin-selective transitions, relative to the long-term homogeneous linewidth, for a subset of centres in the device, allowing us to hyperpolarize the ground state electron just as we did in bulk ^{28}Si at zero-field.

We confirm the ability to hyperpolarize a subset of the sample by observing anti-holes in the hole burning spectrum wherein both of the ground states are being addressed by either the pump or probe lasers. Figure 4(a) shows an example spectrum with anti-holes separated by ~ 12 GHz. We also observe a spectral hole, indicating a subset of centres with sufficiently large B–C overlap to produce a saturation hole. The power dependence (see Fig. 3(a)) is well modelled by Eq. (1) and we observe a minimum instantaneous linewidth of 720 ± 50 MHz. An increase in instantaneous linewidth is to be expected; measuring the hole at field preferentially selects centres with instantaneous linewidth on the order of the B–C splitting, $\Delta_{BC}^{1,2} = \Delta_e^{1,2} - \Delta_g = \{2, 3\}$ GHz, as these centres contribute disproportionately to the single-laser fluorescence. It is also possible that the observed sample strain increases spectral diffusion.

In general we expect anti-holes at pump-probe detunings of $\pm\Delta_g$, $\pm\Delta_{BC}$ and $\pm\Delta_{AD} = \pm(\Delta_g + \Delta_e)$ [62]. The observed ± 6 GHz anti-holes splitting is attributed to Δ_e. We confirm this assessment with a zero-parameter fit of a four level rate equation model included as SI. With this assignment in mind we schematically illustrate the formation of the hole and anti-holes in the insets of Fig. 4(a). A saturation hole is present when both pump and probe are driving the overlap of the B and C transitions. The anti-holes are symmetric about the hole as inhomogeneous broadening will lead to two bright subsets illustrated with solid and dashed ground state levels.

This hole-burning spectrum indicates that a subset of T centre spins can be initialized optically. Additionally, a pulsed pump laser can be used to measure the spin population via the luminescence transient as the spins hyperpolarize from bright to dark states. This is sufficient to measure a T_1 lifetime for this subset [37]. We apply two lasers pulsing at wavelengths λ_1 and λ_2 separated by
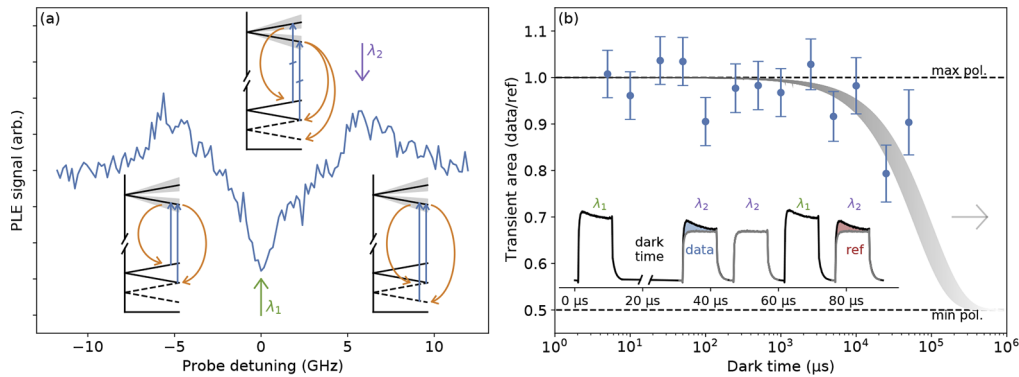
Fig. 4. T$_1$ measurement via hole burning. (a) Hole burning spectrum of the sample at field showing the saturation hole at zero detuning and the anti-holes at detunings equal to the ground state splitting. (Insets) Energy level diagrams schematically illustrating the pump-probe conditions for saturation and anti-holes for two sub-ensembles of the inhomogeneously broadened line (solid and dashed lines in the ground state). At zero detuning the dashes on the upward arrows indicate equal energies. (b) Spin relaxation measured over time bounds the population lifetime $T_1 > 80 \pm 20$ ms as shown by the error bounds of an exponential fit (grey region). (Inset) The pulse sequence of the two lasers tuned to $\lambda_{1,2}$ as shown in (a) along with the measured signal from each pulse showing the hyperpolarization transient. Spin relaxation is determined by the ratio of data (blue) and reference (red) transient areas.

the ground state splitting Δ_e. The pulse scheme and luminescence transients are shown inset to Fig. 4(b). The system is initialized into an out-of-equilibrium spin state in which a sub-ensemble is hyperpolarized by λ_1. After a variable dark time the spin state is read out with two pulses at wavelength λ_2. The first 'readout' pulse will pump between the two electron spin states of the sub-ensemble, leading to a transient luminescence signal. Subsequently probing the system with the same wavelength (λ_2) yields no further hyperpolarization or accompanying transient, but rather only a constant background luminescence signal from the unresolved sub-ensemble. The difference between the integrated luminescence during these pulses is proportional to the spin population in the addressed state. This readout transient (blue) is labeled 'data'. Afterwards, an additional round of initialization and readout is performed without any dark time to give a reference transient (red), labeled 'ref'. The data transient is compared to the reference to get a polarization ratio that drops from 1 (maximally polarized) to 0.5 (no polarization) in thermal equilibrium.

The resulting polarization ratio versus dark time is shown in Fig. 4(b). The shortest spin lifetime (T_1) consistent with the observed polarization data is 60 ms, as determined by fitting a polarization decay curve with a decay time of 80 ± 20 ms indicated by the grey uncertainty region on Fig. 4(b). Finite optical pulse extinction artificially lowers the measurable T_1 as leaked laser light will slowly drive the spins to a mixed state during the dark time. The true T_1 is expected to be substantially larger. Although the measured bound $T_1 > 60$ ms is short compared to the bulk relaxation time, $T_1 > 16$ s [24], it improves on the previous bound for integrated T centres, measured by the same technique in Ref. [37], as expected given higher optical pulse extinction, and it is sufficiently long to measure the electron spin coherence by combining the same optical initialization and readout scheme with microwave control. Future work to increase extinction during the dark time via, eg, additional optical modulators, will be necessary.

8. Discussion

We have integrated the silicon T centre with monolithic photonic waveguides and measured the homogeneous and ensemble properties. Such T centre devices can be efficiently networked on chip with integrated photonic cavities, switches, and detectors [63], as well as efficiently fibre coupled for remote networks. Integrating the T centre with nanophotonics fabricated by a standard, unoptimized commercial CMOS process shows no significant degradation of optical properties compared to the unpatterned chip material.

We measure, for the first time, instantaneous homogeneous T centre linewidths and compare a variety of materials including waveguide-integrated centres and bulk ^{28}Si. Promisingly, we determine instantaneous homogeneous linewidths one to two orders of magnitude better than previously reported spectral diffusion linewidths and show that a nearly transform-limited linewidth is achievable in ^{28}Si. With these instantaneous homogeneous linewidth values we can predict the indistinguishability of networked T centre spin-photon interfaces. With appropriate feedback the slow spectral diffusion can be made negligible and luminescence from two or more emitters with zero relative detuning can be made to interfere [53,54]. In this limit interference visibility is determined only by the emitter lifetimes and the emission linewidth [41]. We predict the interference visibility for T centres in ^{nat}Si waveguides and bulk ^{28}Si (Supplement 1, Table S1). We also tabulate what Purcell factor, F_P, and cavity quality, Q, are necessary to entangle two T centre spins beyond the Bell threshold [64]. A precise determination of the radiative efficiency is critical, but we find high visibility is achievable with demonstrated photonics in every case.

Assuming unit radiative efficiency only $F_P \approx 2,200$ (120), achievable in a nanophotonic cavity of $Q \approx 14,000$ (800), is required for a visibility of 56% based on the lowest measured linewidth (or inferred low-power limit) of waveguide-integrated T centres. If instead we assume the current radiative efficiency bound from experiment, 0.03 [37], $F_P \approx 73,000$ (4000) is needed, requiring a cavity of $Q \approx 480,000$ (27,000). Such quality factors are routine in silicon nanophotonics [65,66]. Centres from the ^{28}Si ensemble could achieve 25% interference visibility without any enhancement, and require only $F_P = 13$ ($F_P = 420$), $Q \approx 83$ (2800), to reach the Bell violation threshold assuming radiative efficiency of 1 (0.03).

Achieving the Purcell factor targets above not only increases entanglement fidelity but also increases emission rate. For waveguide-integrated T centres the emission lifetime is lowered to 2 ns (33 ns) for the lowest measured linewidth (or inferred low-power limit). The ^{28}Si ensemble would have an emission lifetime of 240 ns although with more room for improvement at such a modest Q factor. For technical applications this presents an operation rate of 10–100 MHz. From these values we have shown that the T centre is a competitive spin-photon interface for a modular quantum information network based on long-range emission-based entanglement, with only modest Purcell enhancement and cavity Q-factors necessary for high fidelity, fast operation.

We showcased the ability to optically initialize and readout electron spins within the waveguide T centre ensemble. We used an all-optical pulse sequence to measure spin relaxation and find a bound on T_1 lifetime. This is a crucial first step towards full spin control of waveguide-device integrated T centres, requiring only inclusion of microwave lines for driving the spins directly. Taken together, these new measurements make the T centre an encouraging spin-photon interface for on-chip networks, ready to be deployed in a silicon-based modular quantum information architecture.

Disclosures. A.D., C.B., C.C., A.A., N.A.B., E.R.M., N.R.L.-H., M.R., M.K., A.T.K.K., M.L.W.T., D.B.H. and S.S. are current or recent employees of and/or have a financial interest in Photonic Inc., a quantum technology company. S.R., N.V.A., H.-J.P. declare no competing interests.

Data availability. Data is available on request. Correspondence and requests for materials should be addressed to Stephanie Simmons.

Supplemental document. See Supplement 1 for supporting content.

References

1. C. Monroe, R. Raussendorf, A. Ruthven, K. R. Brown, P. Maunz, L. M. Duan, and J. Kim, "Large-scale modular quantum-computer architecture with atomic memory and photonic interconnects," Phys. Rev. A **89**(2), 022317 (2014).
2. K. Nemoto, M. Trupke, S. J. Devitt, A. M. Stephens, B. Scharfenberger, K. Buczak, T. Nöbauer, M. S. Everitt, J. Schmiedmayer, and W. J. Munro, "Photonic architecture for scalable quantum information processing in diamond," Phys. Rev. X **4**(3), 031022 (2014).
3. P. Lodahl, "Quantum-dot based photonic quantum networks," Quantum Sci. Technol. **3**(1), 013001 (2018).
4. L. J. Stephenson, D. P. Nadlinger, B. C. Nichol, S. An, P. Drmota, T. G. Ballance, K. Thirumalai, J. F. Goodwin, D. M. Lucas, and C. J. Ballance, "High-Rate, High-Fidelity Entanglement of Qubits Across an Elementary Quantum Network," Phys. Rev. Lett. **124**(11), 110501 (2020).
5. M. Pompili, S. L. Hermans, S. Baier, H. K. Beukers, P. C. Humphreys, R. N. Schouten, R. F. Vermeulen, M. J. Tiggelman, L. dos Santos Martins, B. Dirkse, S. Wehner, and R. Hanson, "Realization of a multinode quantum network of remote solid-state qubits," Science **372**(6539), 259–264 (2021).
6. A. Gold, J. P. Paquette, A. Stockklauser, M. J. Reagor, M. S. Alam, A. Bestwick, N. Didier, A. Nersisyan, F. Oruc, A. Razavi, B. Scharmann, E. A. Sete, B. Sur, D. Venturelli, C. J. Winkleblack, F. Wudarski, M. Harburn, and C. Rigetti, "Entanglement across separate silicon dies in a modular superconducting qubit device," npj Quantum Inf. **7**(1), 142 (2021).
7. T. van Leent, M. Bock, F. Fertig, R. Garthoff, S. Eppelt, Y. Zhou, P. Malik, M. Seubert, T. Bauer, W. Rosenfeld, W. Zhang, C. Becher, and H. Weinfurter, "Entangling single atoms over 33 km telecom fibre," Nature **607**(7917), 69–73 (2022).
8. S. T. Ylmaz, P. Fallahi, and A. Imamog, "Quantum-Dot-Spin Single-Photon Interface," Phys. Rev. Lett. **105**(3), 033601 (2010).
9. K. De Greve, L. Yu, P. L. McMahon, J. S. Pelc, C. M. Natarajan, N. Y. Kim, E. Abe, S. Maier, C. Schneider, M. Kamp, S. Höfling, R. H. Hadfield, A. Forchel, M. M. Fejer, and Y. Yamamoto, "Quantum-dot spin-photon entanglement via frequency downconversion to telecom wavelength," Nature **491**(7424), 421–425 (2012).
10. W. B. Gao, P. Fallahi, E. Togan, J. Miguel-Sanchez, and A. Imamoglu, "Observation of entanglement between a quantum dot spin and a single photon," Nature **491**(7424), 426–430 (2012).
11. C. Arnold, J. Demory, V. Loo, A. Lemaître, I. Sagnes, M. Glazov, O. Krebs, P. Voisin, P. Senellart, and L. Lanco, "Macroscopic rotation of photon polarization induced by a single spin," Nat. Commun. **6**(1), 6236 (2015).
12. D. Ding, M. H. Appel, A. Javadi, X. Zhou, M. C. Löbl, I. Söllner, R. Schott, C. Papon, T. Pregnolato, L. Midolo, A. D. Wieck, A. Ludwig, R. J. Warburton, T. Schröder, and P. Lodahl, "Coherent Optical Control of a Quantum-Dot Spin-Qubit in a Waveguide-Based Spin-Photon Interface," Phys. Rev. Appl. **11**(3), 031002 (2019).
13. T. Zhong, J. M. Kindem, J. G. Bartholomew, J. Rochman, I. Craiciu, V. Verma, S. W. Nam, F. Marsili, M. D. Shaw, A. D. Beyer, and A. Faraon, "Optically Addressing Single Rare-Earth Ions in a Nanophotonic Cavity," Phys. Rev. Lett. **121**(18), 183603 (2018).
14. A. M. Dibos, M. Raha, C. M. Phenicie, and J. D. Thompson, "Atomic Source of Single Photons in the Telecom Band," Phys. Rev. Lett. **120**(24), 243601 (2018).
15. M. Raha, S. Chen, C. M. Phenicie, S. Ourari, A. M. Dibos, and J. D. Thompson, "Optical quantum nondemolition measurement of a single rare earth ion qubit," Nat. Commun. **11**(1), 1605 (2020).
16. A. M. Dibos, M. T. Solomon, S. E. Sullivan, M. K. Singh, K. E. Sautter, C. P. Horn, G. D. Grant, Y. Lin, J. Wen, F. J. Heremans, S. Guha, and D. D. Awschalom, "Purcell Enhancement of Erbium Ions in TiO$_2$ on Silicon Nanocavities," Nano Letters (2022).
17. A. Gruber, A. Dräbenstedt, C. Tietz, L. Fleury, J. Wrachtrup, and C. Von Borczyskowski, "Scanning confocal optical microscopy and magnetic resonance on single defect centers," Science **276**(5321), 2012–2014 (1997).
18. S. L. N. Hermans, M. Pompili, H. K. C. Beukers, S. Baier, J. Borregaard, and R. Hanson, "Qubit teleportation between non-neighbouring nodes in a quantum network," Nature **605**(7911), 663–668 (2022).
19. A. L. Falk, B. B. Buckley, G. Calusine, W. F. Koehl, V. V. Dobrovitski, A. Politi, C. A. Zorman, P. X. Feng, and D. D. Awschalom, "Polytype control of spin qubits in silicon carbide," Nat. Commun. **4**(1), 1819 (2013).
20. G. Wolfowicz, C. P. Anderson, B. Diler, O. G. Poluektov, F. Joseph Heremans, and D. D. Awschalom, "Vanadium spin qubits as telecom quantum emitters in silicon carbide," Sci. Adv. **6**(18), 1 (2020).
21. C. Babin, R. Stöhr, and N. Morioka, *et al.*, "Fabrication and nanophotonic waveguide integration of silicon carbide colour centres with preserved spin-optical coherence," Nat. Mater. **21**(1), 67–73 (2022).
22. C. Yin, M. Rancic, G. G. De Boo, N. Stavrias, J. C. McCallum, M. J. Sellars, and S. Rogge, "Optical addressing of an individual erbium ion in silicon," Nature **497**(7447), 91–94 (2013).

23. K. Morse, R. Abraham, A. DeAbreu, C. Bowness, T. Richards, H. Riemann, N. Abrosimov, P. Becker, H.-J. Pohl, M. Thewalt, and S. Simmons, "A photonic platform for donor spin qubits in silicon," Sci. Adv. **3**(7), 1 (2017).

24. L. Bergeron, C. Chartrand, A. T. K. Kurkjian, K. J. Morse, H. Riemann, N. V. Abrosimov, P. Becker, H.-J. Pohl, M. L. W. Thewalt, and S. Simmons, "Silicon-Integrated Telecommunications Photon-Spin Interface," PRX Quantum **1**(2), 020301 (2020).

25. N. Lauk, N. Sinclair, S. Barzanjeh, J. P. Covey, M. Saffman, M. Spiropulu, and C. Simon, "Perspectives on quantum transduction," Quantum Sci. Technol. **5**(2), 020501 (2020).

26. J. Borregaard, A. S. Sørensen, and P. Lodahl, "Quantum Networks with Deterministic Spin–Photon Interfaces," Adv. Quantum Technol. **2**(5-6), 1800091 (2019).

27. C. Beaufils, W. Redjem, E. Rousseau, V. Jacques, A. Y. Kuznetsov, C. Raynaud, C. Voisin, A. Benali, T. Herzig, S. Pezzagna, J. Meijer, M. Abbarchi, and G. Cassabois, "Optical properties of an ensemble of G-centers in silicon," Phys. Rev. B **97**(3), 035303 (2018).

28. M. Prabhu, C. Errando-Herranz, L. De Santis, I. Christen, C. Chen, and D. R. Englund, "Individually Addressable Artificial Atoms in Silicon Photonics," arXiv, arXiv.2202.02342 (2022).

29. J. Yang, W. Fan, Y. Zhang, C. Duan, G. G. De Boo, R. L. Ahlefeldt, J. J. Longdell, B. C. Johnson, J. C. McCallum, M. J. Sellars, S. Rogge, C. Yin, and J. Du, "Zeeman and hyperfine interactions of a single $^{167}Er^{3+}$ ion in Si," Phys. Rev. B **105**(23), 235306 (2022).

30. M. Hollenbach, N. S. Jagtap, C. Fowley, J. Baratech, V. Guardia-Arce, U. Kentsch, A. Eichler-Volf, N. V. Abrosimov, A. Erbe, C. Shin, H. Kim, M. Helm, W. Lee, G. V. Astakhov, and Y. Berencén, "Metal-assisted chemically etched silicon nanopillars hosting telecom photon emitters," J. Appl. Phys. **132**(3), 033101 (2022).

31. C. Chartrand, L. Bergeron, K. J. Morse, H. Riemann, N. V. Abrosimov, P. Becker, H.-J. Pohl, S. Simmons, and M. L. W. Thewalt, "Highly enriched ^{28}Si reveals remarkable optical linewidths and fine structure for well-known damage centers," Phys. Rev. B **98**(19), 195201 (2018).

32. S. Buckley, J. Chiles, A. N. McCaughan, G. Moody, K. L. Silverman, M. J. Stevens, R. P. Mirin, S. W. Nam, and J. M. Shainline, "All-silicon light-emitting diodes waveguide-integrated with superconducting single-photon detectors," Appl. Phys. Lett. **111**(14), 141101 (2017).

33. Y. Baron, A. Durand, P. Udvarhelyi, T. Herzig, M. Khoury, S. Pezzagna, J. Meijer, I. Robert-Philip, M. Abbarchi, J.-M. Hartmann, V. Mazzocchi, J.-M. Gérard, A. Gali, V. Jacques, G. Cassabois, and A. Dréau, "Detection of Single W-Centers in Silicon," ACS Photonics **9**(7), 2337–2345 (2022).

34. I. R. Berkman, A. Lyasota, G. G. D. Boo, J. G. Bartholomew, B. C. Johnson, C. Jeffrey, B.-b. Xu, S. Xie, R. L. Ahlefeldt, M. J. Sellars, C. Yin, and S. Rogge, "Sub-megahertz homogeneous linewidth for Er in Si via in situ single photon detection," arXiv, arXiv.2108.07090 (2021).

35. L. Weiss, A. Gritsch, B. Merkel, and A. Reiserer, "Erbium dopants in nanophotonic silicon waveguides," Optica **8**(1), 40 (2021).

36. E. R. MacQuarrie, C. Chartrand, D. B. Higginbottom, K. J. Morse, V. A. Karasyuk, S. Roorda, and S. Simmons, "Generating T centres in photonic silicon-on-insulator material by ion implantation," New J. Phys. **23**(10), 103008 (2021).

37. D. B. Higginbottom, A. T. K. Kurkjian, and C. Chartrand, *et al.*, "Optical observation of single spins in silicon," Nature **607**(7918), 266–270 (2022).

38. S. D. Barrett and P. Kok, "Efficient high-fidelity quantum computation using matter qubits and linear optics," Phys. Rev. A **71**(6), 060310 (2005).

39. E. Waks and J. Vuckovic, "Dipole induced transparency in drop-filter cavity-waveguide systems," Phys. Rev. Lett. **96**(15), 153601 (2006).

40. J. Kerckhoff, L. Bouten, A. Silberfarb, and H. Mabuchi, "Physical model of continuous two-qubit parity measurement in a cavity-QED network," Phys. Rev. A **79**(2), 024305 (2009).

41. B. Kambs and C. Becher, "Limitations on the indistinguishability of photons from remote solid state sources," New J. Phys. **20**(11), 115003 (2018).

42. J. Bylander, I. Robert-Philip, and I. Abram, "Interference and correlation of two independent photons," Eur. Phys. J. D **22**(2), 295–301 (2003).

43. F. D. Martini, G. Innocenti, G. R. Jacobovitz, and P. Mataloni, "Anomalous Spontaneous Emission Time in a Microscopic Optical Cavity," Phys. Rev. Lett. **59**(26), 2955–2958 (1987).

44. S. Wein, N. Lauk, R. Ghobadi, and C. Simon, "Feasibility of efficient room-temperature solid-state sources of indistinguishable single photons using ultrasmall mode volume cavities," Phys. Rev. B **97**(20), 205418 (2018).

45. A. N. Safonov, E. C. Lightowlers, G. Davies, P. Leary, R. Jones, and S. Öberg, "Interstitial-Carbon Hydrogen Interaction in Silicon," Phys. Rev. Lett. **77**(23), 4812–4815 (1996).

46. N. S. Minaev and A. V. Mudryi, "Thermally-induced defects in silicon containing oxygen and carbon," Phys. Stat. Sol. (a) **68**(2), 561–565 (1981).

47. D. Dhaliah, Y. Xiong, A. Sipahigil, S. M. Griffin, and G. Hautier, "First-principles study of the T center in silicon," Phys. Rev. Mater. **6**(5), L053201 (2022).

48. Y. Wang, W. Shi, X. Wang, Z. Lu, M. Caverley, R. Bojko, L. Chrostowski, and N. A. F. Jaeger, "Design of broadband subwavelength grating couplers with low back reflection," Opt. Lett. **40**(20), 4647–4650 (2015).

49. A. N. Safonov, E. C. Lightowlers, and G. Davies, "Carbon-hydrogen deep level luminescence centre in silicon responsible for the T-line," Mater. Sci. Forum **196-201**, 909–914 (1995).

50. A. Goban, C.-L. Hung, J. Hood, S.-P. Yu, J. Muniz, O. Painter, and H. Kimble, "Superradiance for Atoms Trapped along a Photonic Crystal Waveguide," Phys. Rev. Lett. **115**(6), 063601 (2015).

51. D. M. Lukin, M. A. Guidry, J. Yang, M. Ghezellou, S. D. Mishra, H. Abe, T. Ohshima, J. Ul-Hassan, and J. Vučković, "Optical superradiance of a pair of color centers in an integrated silicon-carbide-on-insulator microresonator," arXiv, arXiv.2202.04845 preprint (2022).

52. N. Kalb, P. C. Humphreys, J. J. Slim, and R. Hanson, "Dephasing mechanisms of diamond-based nuclear-spin memories for quantum networks," Phys. Rev. A **97**(6), 062330 (2018).

53. V. M. Acosta, C. Santori, A. Faraon, Z. Huang, K.-M. C. Fu, A. Stacey, D. A. Simpson, K. Ganesan, S. Tomljenovic-Hanic, A. D. Greentree, S. Prawer, and R. G. Beausoleil, "Dynamic Stabilization of the Optical Resonances of Single Nitrogen-Vacancy Centers in Diamond," Phys. Rev. Lett. **108**(20), 206401 (2012).

54. H. Bernien, L. Childress, L. Robledo, M. Markham, D. Twitchen, and R. Hanson, "Two-Photon Quantum Interference from Separate Nitrogen Vacancy Centers in Diamond," Phys. Rev. Lett. **108**(4), 043604 (2012).

55. A. E. Siegman, *Lasers* (University Science Books, Sausalito California, 1986).

56. C. P. Anderson, A. Bourassa, K. C. Miao, G. Wolfowicz, P. J. Mintun, A. L. Crook, H. Abe, J. U. Hassan, N. T. Son, T. Ohshima, and D. D. Awschalom, "Electrical and optical control of single spins integrated in scalable semiconductor devices," Science **366**(6470), 1225–1230 (2019).

57. S. B. Van Dam, M. Walsh, M. J. Degen, E. Bersin, S. L. Mouradian, A. Galiullin, M. Ruf, M. Ijspeert, T. H. Taminiau, R. Hanson, and D. R. Englund, "Optical coherence of diamond nitrogen-vacancy centers formed by ion implantation and annealing," Phys. Rev. B **99**(16), 161203 (2019).

58. A. Berthelot, I. Favero, G. Cassabois, C. Voisin, C. Delalande, Ph. Roussignol, R. Ferreira, and J. M. Gérard, "Unconventional motional narrowing in the optical spectrum of a semiconductor quantum dot," Nat. Phys. **2**(11), 759–764 (2006).

59. G. Sallen, A. Tribu, T. Aichele, R. André, L. Besombes, C. Bougerol, M. Richard, S. Tatarenko, K. Kheng, and J. -Ph. Poizat, "Subnanosecond spectral diffusion measurement using photon correlation," Nat. Photonics **4**(10), 696–699 (2010).

60. Z. Ciechanowska, G. Davies, and E. C. Lightowlers, "Uniaxial stress measurements on the 1039.8 meV zero-phonon line in irradiated silicon," Solid State Commun. **49**(5), 427–431 (1984).

61. A. M. Stoneham, "Shapes of Inhomogeneously Broadened Resonance Lines in Solids," Rev. Mod. Phys. **41**(1), 82–108 (1969).

62. M. Nilsson, L. Rippe, S. Kröll, R. Klieber, and D. Suter, "Hole-burning techniques for isolation and study of individual hyperfine transitions in inhomogeneously broadened solids demonstrated in Pr^{3+}:Y_2SiO_5," Phys. Rev. B **70**(21), 214116 (2004).

63. M. K. Akhlaghi, E. Schelew, and J. F. Young, "Waveguide integrated superconducting single-photon detectors implemented as near-perfect absorbers of coherent radiation," Nat. Commun. **6**(1), 8233 (2015).

64. B. Hensen, H. Bernien, A. Dreau, A. Reiserer, N. Kalb, M. S. Blok, J. Ruitenberg, R. F. L. Vermeulen, R. N. Schouten, C. Abellan, W. Amaya, V. Pruneri, M. W. Mitchell, M. Markham, D. J. Twitchen, D. Elkouss, S. Wehner, T. H. Taminiau, and R. Hanson, "Loophole-free Bell inequality violation using electron spins separated by 1.3 kilometres," Nature **526**(7575), 682–686 (2015).

65. K. Ashida, M. Okano, M. Ohtsuka, M. Seki, N. Yokoyama, K. Koshino, M. Mori, T. Asano, S. Noda, and Y. Takahashi, "Ultrahigh-Q photonic crystal nanocavities fabricated by CMOS process technologies," Opt. Express **25**(15), 18165 (2017).

66. P. B. Deotare, M. W. McCutcheon, I. W. Frank, M. Khan, and M. Lončar, "High quality factor photonic crystal nanobeam cavities," Appl. Phys. Lett. **94**(12), 121106 (2009).